information

MDPI

Article

The Diffraction Research of Cylindrical Block Effect Based on Indoor 45 GHz Millimeter Wave Measurements

Xingrong Li *, Yongqian Li and Baogang Li

Department of Electronic and Communication Engineering, North China Electric Power University, Baoding 071003, China; liyq@ncepu.edu.cn (Y.L.); baogangli@ncepu.edu.cn (B.L.)

* Correspondence: li-xingrong@163.com; Tel.: +86-0312-7522624

Academic Editors: Lei Chen, Wenjia Li and Rami J. Haddad

Received: 3 April 2017; Accepted: 27 April 2017; Published: 2 May 2017

Abstract: In this paper, four kinds of block diffraction models were proposed on the basis of the uniform geometrical theory of diffraction, and these models were validated by experiments with 45 GHz millimeter wave in the laboratory. The results are in agreement with the theoretical analysis. Some errors exist in the measurement results because of the unsatisfactory experimental environment. Single conducting cylindrical block measurement error was less than 0.5 dB, and single man block measurement error in the school laboratory was less than 1 dB, while in the factory laboratory environment, the peak to peak error reached 1.6 dB. Human body block attenuation was about 5.9–9.2 dB lower than that of the single conducting cylinder. A human body and a conducting cylinder were used together as a block in model (c) and model (d), but the positions of the cylinder in the two models were different. The measurement results showed that the attenuation of model (d) is about 3 dB higher than that of model (c).

Keywords: cylindrical block; 45 GHz millimeter wave; uniform geometrical diffraction model; communication measurement

1. Introduction

Exploiting new spectrums for cellular communication to boost its capacity to Gigabit is the main issue faced by the next generation (5G) of mobile communication [1,2], and is considered a problem of wide concern. Millimeter wave frequency band has abundant bandwidth resources which can be utilized to solve this problem.

The cylindrical block is very common, in which a millimeter wave signal becomes seriously decayed. The blocking effect of the human body is one of the key issues to be considered in millimeter wave communication. The loss from multiple human blockers is investigated at millimeter wave frequencies. The blocking effect as absorbing screens of infinite height with two knife-edges was modelled, and a physical optics approach was used to compute the diffraction around the absorbing screens [3]. Some scholars have studied the human block effect on 26 GHz and 39 GHz millimeter waves in laboratory environments. The experiment results show that the human body block in an indoor environment will cause a very high loss to the transmission link [4,5]. Penetration loss caused by wood and glass with different thicknesses and surfaces, as well as signal attenuation caused by trees were also measured in [5].The attenuation of an indoor wireless channel at 60 GHz has also been reported in [6,7]. In the literature [8], P.H. Pathak and his colleague analyzed the diffraction of electromagnetic waves by a smooth convex surface, and deduced the relative diffraction parameters under the condition that the signal source is on the surface or blocked. Several scholars reported the diffraction and scattering of a high frequency wave by a cylinder block [9,10]. An approximate

model was proposed in [11], in which an indoor human body was substituted by a conducting circular cylinder at microwave frequencies. Several scientists have analyzed the curved edge diffraction and wedge diffraction, and deduced the received electric field in the shadow region [12,13]. In the literature [14], a new heuristic approach for multiple edge diffraction modeling based on the uniform theory of diffraction (UTD) was proposed. Professor C. Tzaras presented a new formulation of the UTD in [15], and the novel solution seems to be superior in terms of computation time and complexity, while achieving very accurate results. Edge diffraction is an important issue in millimeter communication. In [16], Vogler presented an attenuation function for multiple knife-edge diffraction, which has been validated by experiments.

In this paper, four kinds of 45 GHz millimeter wave cylindrical block measurement models were proposed. A series of measurements identifying the signal attenuation at 45 GHz under the cylindrical and human body block were carried out. The diffraction properties of a 45 GHz millimeter wave under the cylinder and human body block were studied by comparing the experimental results with the theoretical simulation results.

2. Experimental Environment and Measurement Model

The diffraction experiments of a 45 GHz millimeter wave under the cylindrical block were carried out in a factory laboratory. The experimental scenario is shown in Figure 1.

Figure 1. Experimental scene.

An arbitrary waveform generator and spectrum analyzer from Agilent Co. were utilized in the experiments. The transmitter (TX) and receiver (RX) adopted directional horn antennas; the positions of the two antennas were kept immobile during the measurements, and the distance between the two antennas was 8.5 m. The experiment system parameters are shown in Table 1.

Table 1. Specification of the system.

Parameter	Value
Carrier	45 GHz
TX power	0 dB
Height of the TX/RX	1.2 m/1.2 m
Gain of the horn antenna	25 dB
Polarization of the horn	vertical
Half Power Beam Width (HPBW) of the horn	10°

Four kinds of block diffraction models were proposed on the basis of the uniform geometrical theory of diffraction, as shown in Figure 2.

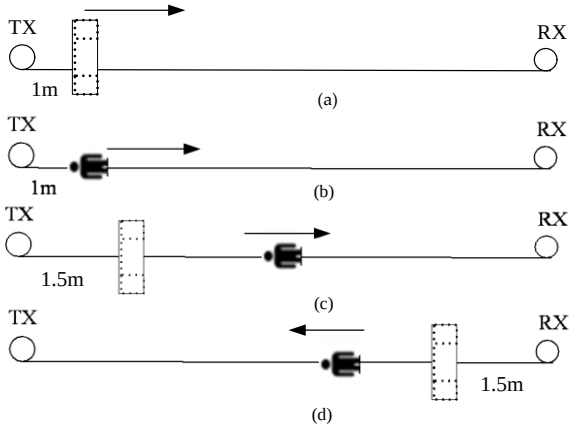

Figure 2. Cylinder and human body block models: (**a**) A cylinder moved along the TX-RX line; (**b**) A man moved along the TX-RX line; (**c**) A cylinder and a moved man blocking the TX-RX connection; (**d**) A moved man and a cylinder blocking the TX-RX connection.

Model (a) is a conducting cylinder made up of four buckets full of water with a diameter of 30 cm (or five metal paint buckets with a diameter of 26 cm). The height of the cylinder is 1.5 m. The cylinder was moved slowly from transmitting antenna to receiving antenna along the connection between them.

Model (b) is a man with a height of 170 cm and a shoulder width of 47 cm. The man moved slowly between the antennas.

Model (c) was composed by a person and a cylinder. The cylinder was fixed at a position about 1.5 m from the transmitting antenna, and the person moved slowly between the cylinder and the receiving antenna.

Model (d) is similar to model (c), but set up in a mirror image with respect to the position of the cylinder and the direction in which the man moves. These models were measured with 45 GHz millimeter wave in our laboratory.

3. Diffraction Theory

3.1. Uniform Theory of Diffraction

The physical model of cylindrical surface diffraction is shown in Figure 3.

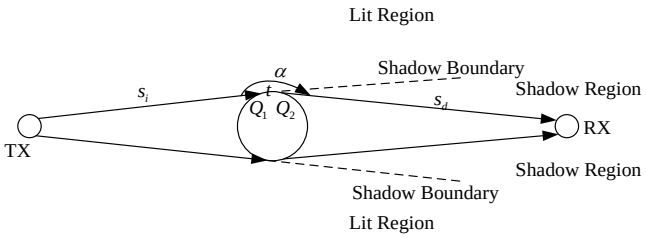

Figure 3. Physical model of cylindrical surface diffraction.

In Figure 3, TX represents the transmitter and RX represents the receiver. The incident ray from the TX at grazing launches a set of surface rays which propagate along a geodesic path on the convex surface, thereby carrying energy into the shadow region. The field associated with these surface rays attenuates due to a continuous shedding or diffraction of rays from the surface rays along the forward tangents to the geodesic surface ray paths [8]. So, the RX in the shadow region can receive the signal sent by the TX.

Uniform geometrical theory of diffraction is considered to be the most suitable solution for engineering planning in cellular communication and broadcasting. According to the UTD theory, the electric field strength behind the block is given by [12]:

$$E = [E_i D(\alpha) + \frac{\partial E_i}{\partial n} d_s(\alpha)] A(s) e^{-jks_d} \tag{1}$$

where E_i is the incident field, $D(\alpha)$ is the amplitude diffraction coefficient, α is the angle between the incident and the diffracted ray as given in Figure 3, k is the wave number, and $A(s)$ is the spreading factor. $d_s(\alpha)$ is the slope diffraction component given by Equation (2):

$$d_s(\alpha) = \frac{1}{jk} \frac{\partial D(\alpha)}{\partial \alpha} \tag{2}$$

The models proposed in this paper can be considered as a far field measurement, because $s_{i,d} >> R$ and $s_{i,d} >> t$, where s_i is the distance of the incident ray, s_d is the distance of the diffracted ray, R is the radius of the cylinder, and t is the distance between Q_1 and Q_2 in Figure 3. According to [14,15], The received signal strength in the shadow region can be expressed as:

$$E(P_s) = E(Q_1) \mathrm{T}_{s,h} A(s_d) e^{-jks_d} \tag{3}$$

where

$$A(S) = \sqrt{\frac{s_i}{s_d(s_i + s_d)}} \tag{4}$$

$$D(\alpha) \approx -0.5\sqrt{L} sign(\alpha) \tag{5}$$

$$L = \frac{s_i s_d}{s_i + s_d} \tag{6}$$

The detailed process of the formula was shown in the literature [14,15].

3.2. Vogler Multiple Knife-Edge Diffraction Theory

Knife-edge diffraction is another issue to be considered. Figure 4 shows the geometry associated with the multiple knife-edge diffraction problem.

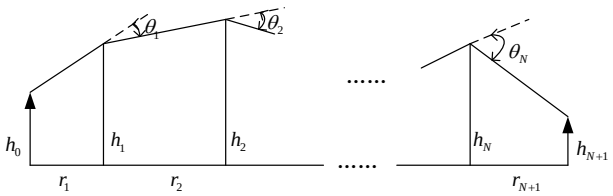

Figure 4. Geometry for multiple knife-edge diffraction.

$\theta_1, \theta_2 \ldots, \theta_N$ are the diffraction angles, $r_1, r_2 \ldots, r_{N+1}$ are the distances of N knife-edges, $h_1, h_2 \ldots, h_N$ are the heights of the knife-edges, h_0 and h_{N+1} are the heights of the transmitter and the receiver, respectively. In [16], an attenuation function for multiple knife-edge diffraction was deduced by Vogler. The attenuation of field strength relative to free space, A, over a path of total distance r_T, and consisting of N knife-edges may be expressed as:

$$\begin{gathered} A = (1/2^N) C_N e^{\sigma N} (2/\sqrt{\pi})^N \\ \int_{\beta_1}^{\infty} \cdots \int_{\beta_N}^{\infty} e^{2f} \cdot e^{-(x_1^2 + x_2^2 + \cdots + x_N^2)} dx_1 \cdots dx_N \end{gathered} \tag{7}$$

where

$$f = \begin{cases} 0, N = 1 \\ \sum_{m=1}^{N-1} \alpha_m (x_m - \beta_m)(x_{m+1} - \beta_{m+1}) \quad N \geq 2 \end{cases} \tag{8}$$

$$\sigma_N = \beta_1^2 + \cdots + \beta_N^2 \tag{9}$$

$$C_N = \begin{cases} 1, N = 1 \\ [\frac{r_2 r_3 \cdots r_N r_T}{(r_1+r_2)(r_2+r_3)\cdots(r_N+r_{N+1})}]^{1/2} \quad N \geq 2 \end{cases} \tag{10}$$

$$r_T = r_1 + r_2 + \cdots + r_{N+1} \tag{11}$$

$$\alpha_m = [\frac{r_m r_{m+2}}{(r_m + r_{m+1})(r_{m+1} + r_{m+2})}]^{1/2} \quad , \quad m = 1, 2, \cdots, N-1 \tag{12}$$

$$\beta_m = \theta_m [\frac{ikr_m r_{m+1}}{2(r_m + r_{m+1})}]^{1/2} \quad m = 1, 2, \cdots, N \tag{13}$$

When $N = 1$, it will be single knife-edge diffraction, and thus Equations (7) and (13) can be simplified as:

$$A = \frac{1}{2} e^{\beta_1^2} \frac{2}{\sqrt{\pi}} \int_{\beta_1}^{\infty} e^{-x^2} dx \tag{14}$$

$$\beta_1 = \theta_1 \sqrt{\frac{ikr_1 r_2}{2(r_1 + r_2)}} \tag{15}$$

where, $k = 2\pi/\lambda$ is the wave number, and i is the imaginary number. The detailed process of the formula was shown in the literature [16].

4. Experiment Results and Analysis

4.1. Experiment Results and Error Analysis

During the experiments, the transmitter and receiver as well as the surrounding objects remained immobile; only the block moved slowly, so the disturbance introduced by the surrounding environment was relatively fixed. In the measurements, channel realizations were measured 10 times at each position, then the mean value was calculated to prevent position randomness and any possible instability of the measurement system.

When the model (a) was measured, the cylinder began to move slowly from the distance of 0.5 m to the distance of 8 m from the transmitter. The measured data are compared with the simulation results, as shown in Figure 5.

According to Figure 5a, the measurement results are very close between the water-filled plastic bucket cylinder and the metal bucket cylinder, which indicates that the 45 GHz millimeter wave has similar diffraction characteristics with each of these cylinders. In the curves, there is an obvious sudden change at 4 m, which should be caused by the multipath effect in the laboratory environment. With multipath propagation, at some measured point the inverse phase signal superposition will cause deep attenuation, and at another measured point the signal will strengthen due to the in-phase signal superposition. In the experiments, small fluctuations occurred at many positions, but they were not so serious as 4 m. In another experiment environment, namely, the school laboratory, the sudden change did not occur, so it can be confirmed that the sudden change at 4 m in the abovementioned experiments was an accidental phenomenon rather than a universal phenomenon. Error analysis is shown in Figure 5b, compared with the theoretical simulation results, and except for the point of 4 m, the measurement error at all other positions is less than 0.5 dB. The results of the measurements are thus in agreement with the theoretical simulation results.

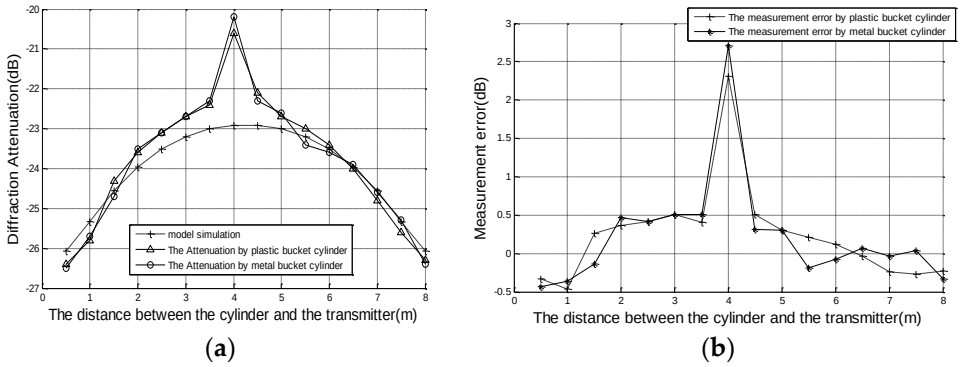

(**a**) (**b**)

Figure 5. Measurement results and error curves under two cylinder blocks of different materials: (**a**) Measurement results and theoretical simulation curves under one cylinder block; (**b**) Error analysis of two cylinder blocks measurement results.

The measurements of the model (b) were carried out in the school laboratory and the factory laboratory, respectively. The measured results and the theoretical simulation results are shown in Figure 6.

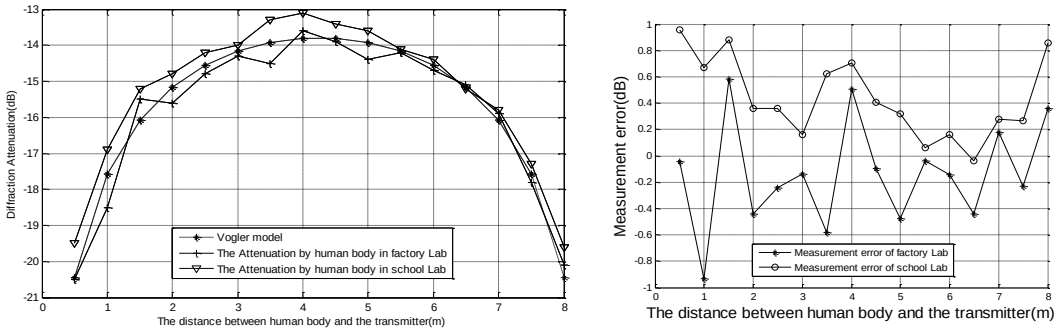

(**a**) (**b**)

Figure 6. Measurement results and error curves under the human body block: (**a**) Measurement results and theoretical simulation under the human body block; (**b**) Error analysis of two laboratory measurement results.

The school laboratory environment proved to be better than the factory laboratory environment, as illustrated in in Figure 1. There was less multipath interference caused by the environment around the transmission pass at the school laboratory.

From Figure 6a, the data measured in the school laboratory is generally larger than the theoretical simulation results. This could be caused by system errors. However, the data measured in the factory laboratory have obvious fluctuations, i.e., the experimental environment has a great impact on the measurement results. The measurement error curves from the two laboratories are shown in Figure 6b. The error in the school laboratory fluctuates between 0 and 1 dB, which can be reduced by improving the accuracy of the experimental system. However, although the consistency of the measurement results in the factory laboratory was poor, its peak-to-peak error is about 1.6 dB.

Comparing the measurement results between model (a) and (b), and by subtracting the cylinder measurement results from the human body measurement results, the differences between them are shown in Figure 7.

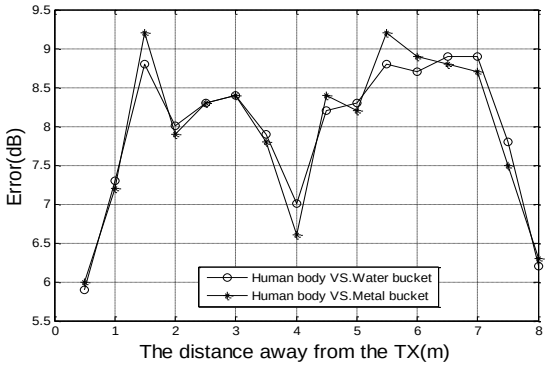

Figure 7. Comparing the measurement results between the human body and the cylinders.

From Figure 7, it is obvious that the 45 GHz millimeter wave signal attenuation by a single body blocking is smaller than that of the single conductor cylinder blocking; the difference between them is 5.9–9.2 dB. Most of the differences between them are larger than 8 dB, even at the closest point to the antenna the difference is approximate 6 dB. Therefore, it can be concluded that the diffraction performance of the human body is better than that of the conductor cylinder for the 45 GHz millimeter wave signal.

The measurement results of model (c) and model (d) are shown in Figure 8.

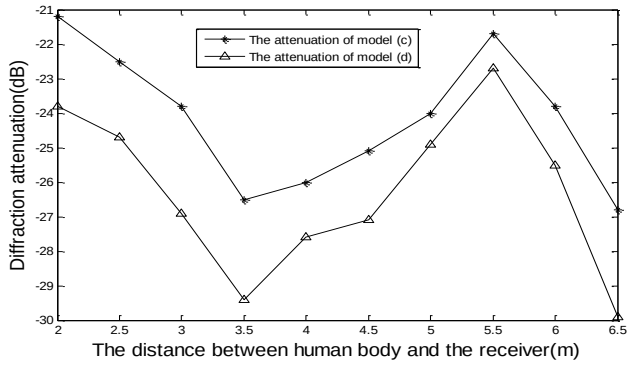

Figure 8. Attenuation measurements of model (c) and model (d).

Comparing the measured data of model (c) and model (d), it is found that their curves are similar, although the attenuation of model (c) is smaller than that of model (d). The biggest difference between them is about 3 dB. This is because when the ray was diffracted by the cylindrical block in model (c), it produced a diffraction angle, and as a person approached the cylinder, due to the diffraction angle, the body was in the shadow region, so its impact on the signal transmission is small. In model (d), the ray penetrated through the human body, and then continued to be blocked by the cylinder, i.e., the human body and the cylinder simultaneously played a blocking role in this model, so the signal attenuation is greater than that of model (c).

For the second peak, when the human body was further away from the cylinder, the peak can be interpreted as follows. According to Vogler single knife-edge diffraction model, in model (c) the scattered signal from the cylinder can be taken as the signal source, and the human body can be analyzed as a single block. When the block is near the middle position between the transmitting antenna and the receiving antenna, the diffraction angle is the least, and the signal attenuation is the smallest. The second peak is near the midpoint between the cylinder and the receiving antenna. In model (d), the result is inverse. These results are consistent with the theory.

4.2. Coverage Analysis

To account for cellular coverage, the attenuation between the transmitter and the receiver must be considered. In the measurements, the power of the transmitter was 0 dBm. When the cylinder or human body was near each antenna, the channel loss was large, i.e., the coverage area was small. When the cylinder or human body was far away from the antennas, the channel properties improved, and the coverage area became larger.

For models (a) and (b), when the block was near each antenna, the received signal power at the position of 10 m from the transmitter was lower than −101 dBm, according to the standard for (Long Term Evolution) LTE coverage, and the 45 GHz millimeter wave cellular coverage radius was about 10 m. When the block was at the midpoint of the antenna connection, the channel characteristics improved, and the received signal power at 13 m was −95.6 dBm, i.e., the 45 GHz millimeter wave cellular coverage radius was more than 13 m.

For models (c) and (d), the signal attenuation in the transmission path was larger than those of models (a) and (b), and the average signal power along the transmission path was less than −85 dBm. When the block was near each antenna, the measured signal power at 8.5 m away from the transmitter was less than −96 dBm, thus the communication quality could not be guaranteed, as the coverage radius of these models was about 9 m.

5. Conclusions

Four kinds of cylinder block models were proposed based on UTD theory and multiple knife-edge diffraction theory. The experiments based on the 45 GHz millimeter wave were carried out to measure the channel attenuation characteristics and cellular coverage radius. Compared with the theoretical simulation, the single conductor cylinder block measurement error was less than 0.5 dB, and single human body block measurement error in school laboratory was less than 1 dB, which can be reduced by improving the accuracy of the experimental system. However, the consistency of the measurement results in the factory laboratory environment was poor, and the peak-to-peak error reached 1.6 dB. The single human block attenuation was about 5.9–9.2 dB lower than that of the single conductor cylinder, while most of the differences between them were greater than 8 dB. The attenuation of model (c) was smaller than that of model (d); the biggest difference between them was about 3 dB. The coverage radius of models (a) and (b) can be more than 15 m in an ideal state, and less than 10 m under poor conditions. The coverage radius of models (c) and (d) was about 9 m. These results are useful for estimating the attenuation and coverage radius of millimeter wave signals in environments with cylindrical and human body obstacles.

Acknowledgments: This work is supported by the National Natural Science Foundation of China (Grants No. 61377088 and 61501185) and Beijing Natural Science Foundation (Grants No. 4164101) and the Fundamental Research Funds for the Central Universities (Grants No. 2015 MS101).

Author Contributions: Xingrong Li proposed the idea and wrote this paper; Xingrong Li and Yongqian Li conceived and carried out the experiments; Xingrong Li and Baogang Li analyzed the data; all authors have read and approved the final manuscript.

Conflicts of Interest: The authors declare no conflict of interest.

References

1. Fettweis, G.; Alamouti, S. 5G: Personal Mobile Internet beyond What Cellular Did to Telephony. *IEEE Commun. Mag.* **2014**, *52*, 140–145. [CrossRef]
2. Thompson, J.; Ge, X.; Wu, H.C.; Irmer, R.; Jiang, H.; Fettweis, G.; Alamouti, S. 5G Wireless Communication Systems: Prospects and Challenges. *IEEE Commun. Mag.* **2014**, *52*, 62–64. [CrossRef]
3. Lu, J.; Steinbach, D.; Cabrol, P.; Pietraski, P. Modeling the Impact of Human Blockers in Millimeter Wave Radio Links. Available online: http://www.interdigital.com/research_papers/2012_01_25_modeling_the_impact_of_human_blockers_in_millimeter_wave_radio_links (accessed on 28 April 2017).

4. Wang, Q.; Zhao, X.; Li, S.; Wang, M.; Sun, S.; Hong, W. Attenuation by a Human Body and Trees as well as Material Penetration Loss in 26 and 39 GHz Millimeter Wave Bands. *Int. J. Antennas Propag.* **2017**, *2017*, 2961090. [CrossRef]
5. Geng, S.Y.; Li, X.; Wang, Q.; Wang, G.B.; Wang, M.J.; Sun, S.H.; Wei, H.; Zhao, X.W. Research on human blockage effect for indoor 26 GHz mm-wave communications. *J. Commun.* **2016**, *37*, 68–73. (In Chinese)
6. Geng, S.Y.; Liu, S.Y.; Hong, W.; Zhao, X.W. Mm-wave 60GHz indoor channel parameters and correlation properties. *Chin. J. Radio Sci.* **2015**, *30*, 808–813. (In Chinese)
7. Jacob, M.; Priebe, S.; Dickhoff, R.; Kleine-Ostmann, T.; Schrader, T.; Kurner, T. Diffraction in mm and sub-mmwave indoor propagation channels. *IEEE Trans. Microw. Theory Tech.* **2012**, *60*, 833–844. [CrossRef]
8. Pathak, P.H.; Burnside, W.; Marhefka, J.R. A uniform GTD analysis of the diffraction of electromagnetic waves by a smooth convex surface. *IEEE Trans. Antennas Propag.* **1980**, *28*, 631–642. [CrossRef]
9. Pathak, P.H. An asymptotic analysis of the scattering of plane waves by a smooth convex cylinder. *Radio Sci.* **1979**, *14*, 419–435. [CrossRef]
10. Idemen, M.I. Diffraction of an Obliquely Incident High-Frequency Wave by a Cylindrically Curved Sheet. *IEEE Trans. Antennas Propag.* **1986**, *34*, 181–187. [CrossRef]
11. Ghaddar, M.; Talbi, L.; Denidni, T.A.; Sebak, A. A Conducting Cylinder For Modeling Human Body Presence in Indoor Propagation Channel. *IEEE Trans. Antennas Propag.* **2007**, *55*, 3099–3103. [CrossRef]
12. Andersen, J.B. UTD Multiple-Edge Transition Zone Diffraction. *IEEE Trans. Antennas Propog.* **1997**, *45*, 1093–1097. [CrossRef]
13. Kouyoumjian, R.G.; Pathak, P.H. A Uniform Geometrical Theory of Diffraction for an Edge in a Perfectly Conducting Surface. *Proc. IEEE* **1974**, *62*, 1448–1461. [CrossRef]
14. Tzaras, C.; Saunders, S.R. An improved heuristic UTD solution for multiple edge transition zone diffraction. *IEEE Trans. Antennas Propag.* **2001**, *49*, 1678–1682. [CrossRef]
15. Koutitas, G.; Tzaras, C. A UTD Solution for Multiple Round Surfaces. *IEEE Trans. Antennas Propag.* **2006**, *54*, 1277–1283. [CrossRef]
16. Vogler, L.E. An attenuation function for multiple knife edge diffraction. *Radio Sci.* **1982**, *17*, 1541–1546. [CrossRef]